DESIGN, CONSTRUCTION AND TEST OF A TWO-STAGE PLANETARY TRACTION SPEED REDUCER

Eduardo Lobo Lustosa Cabral
Escola Politécnica da Universidade de São Paulo
Departamento de Engenharia Mecatrônica e Sistemas Mecânicos
Av. Mello Moraes, 2231
elcabral@usp.br

Fabrício Sunahara Nagahashi
Escola Politécnica da Universidade de São Paulo
Departamento de Engenharia Mecatrônica e Sistemas Mecânicos
Av. Mello Moraes, 2231
fsnaga@uol.com.br

Marcos Costa Hunold
Escola Politécnica da Universidade de São Paulo
Departamento de Engenharia Mecatrônica e Sistemas Mecânicos
Av. Mello Moraes, 2231
mahunold@usp.br

Abstract. *This work presents the design and test of a two-stage planetary traction speed reducer. This is a precision reducer that presents low speed and torque fluctuations, low vibration level, and zero backlash. This reducer does not have gears, transmission is made by the friction between smooth surfaces, which enables the reducer to have zero backlash. A traction fluid is used forming a film pad between the surfaces avoiding the metal-to-metal contact. Theoretical studies concerning the principles of movement and torque transmission, the Hertz contact stresses, and the contact fatigue criteria are performed. The Hertz contact stresses combined with the contact fatigue criterion are used to predict the life of the reducer. The reducer's configuration, working principle, kinematics and force analysis are described. Finally, tests are performed to determine the reducer precision. These tests are based on measurements of angular transmission error, velocity fluctuation, torsional stiffness and backlash. Results of the angular transmission error and backlash permitted to conclude that the reducer could be classified as a precise device.*

Keywords: planetary drive, traction drive, contact stresses, position accuracy.

1. Introduction

Many industrial types of machines require high precision transmission systems. The angular speed reducers are among the most used devices for this end. The characteristics that determine the precision of a speed reducer are: low torque and speed fluctuation; high torsional stiffness; zero backlash; and low vibration level.

Today the speed reducers most used in high precision machines are: worm and gear, harmonic, traction, and cycloidal. Worm and gear reducers present low efficiency and high wear of the teeth that reduce its life. The precision cycloidal reducers are very expensive because the gears profile is difficult to manufacture with the required precision and surface roughness. The harmonic drivers present the highest torque to weight relation among all the others speed reducers, however they have low stiffness. All these reducers have a common drawback, they are made by gears, which inevitably causes backlash and speed fluctuations limiting their use in high precision systems.

A traction speed reducer does not have teeth; the movement and torque transmission is performed by the friction between two surfaces separated by a film of a special lubricant fluid. This kind of transmission eliminates backlash, thus improving the precision of the system. Also the absence of teeth decreases the torque and speed fluctuations, as well as noise and vibration level. Therefore, the traction reducers present several advantages over the other types of reducers in almost all the aspects that determine precision.

A traction transmission is characterized by the presence of a fluid film pad between the solid surfaces impeding the metal-to-metal contact. The metal-to-metal contact must be avoided to prevent surface damage. The torque and movement are transmitted from one surface to the other by the fluid film shear resistance. The fluid in the space between the two surfaces is submitted to high compression forces. The traction fluids have the property to increase their viscosity several times when they are submitted to high pressures.

The traction coefficient defined as the relation between the tangential and the normal forces between two surfaces separated by a fluid film is the most important design parameter for a traction speed reducer. Its value together with the required maximum torque determines the pre-load forces (normal forces), the reducer life and the size of the reducer's parts. According to Kraus (1992) the traction coefficient provided by a given fluid depends on several parameters involved in the transmission, such as: contact pressure, temperature, surface velocities, and contact geometry. The most used traction fluid for transmissions is the Santotrac-50, which provides the highest traction coefficient among all the traction fluids available according to a comprehensive study made by Kraus (1992) and Loewenthal and Rohn (1985).

2. The two-stage planetary traction speed reducer

The two-stage planetary traction speed reducer present in this paper consists on an improvement over other designs developed by Cisneros (1996) and Hunold (1999). Cisneros (1996) developed a composed two-stage planetary traction reducer. The transmission ration of this reducer was 1:81, and it had the uniqueness to be very compact, but its pre-load system was based on geometric interference between the reducer elements, thus making the assembly process difficult. Hunold (1999) developed a single stage planetary traction reducer with a transmission ratio of 1:9, which had essentially the same design characteristics of the two-stage reducer presented in this paper.

The two-stage planetary traction speed reducer is shown schematically in Fig. (1). The two stages are composed by a "sun", three "planets", a external ring, and a "arm". The reducer input shaft is the sun of the first stage. The operation of both stages is similar. The sun transmits torque and movement to the planets. The external ring is fixed. The planets are in contact with the sun and the external ring, so as the sun rotates the planets rotates and their centers describe a circular trajectory around the sun. The planets axes are connected to the arm. The arm of the first stage is fixed with the sun of the second stage, and the arm of the second stage is the output shaft.

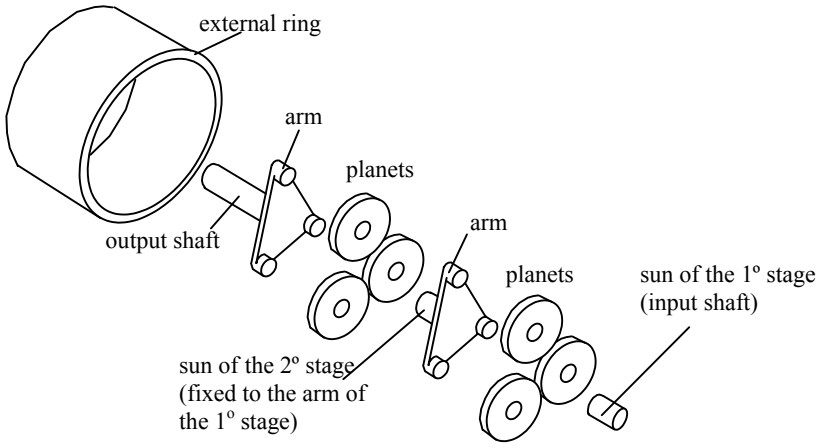

Figure 1. Schematic of the two-stage planetary traction speed reducer.

The dimensions of the sun, planets, and external ring are adopted to be the same for both stages. Therefore, in the kinematics analysis that follows this adoption is implicit.

2.1. Kinematics analysis

The relations among the diameters of the sun, planets an external rings are determined by the desired transmission ratio through a kinematics analysis. Figure (2) shows a frontal view of one stage of the planetary reducer.

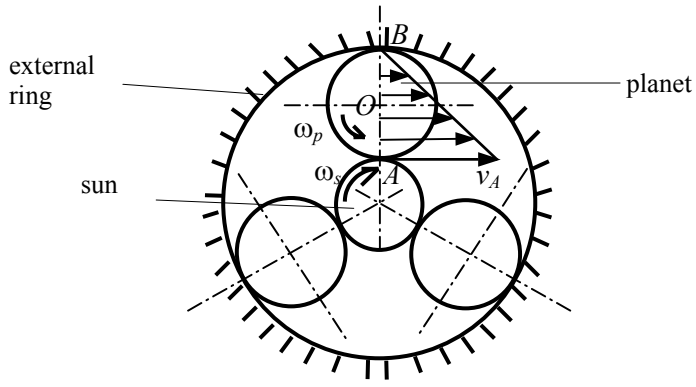

Figure 2. Frontal view of one stage of the planetary traction reducer.

Since point *B* is an instantaneous center of rotation its linear velocity is zero, thus, from simple kinematics considerations the velocity of point *A* (v_A) is given by:

$$v_A = \omega_S \frac{d_S}{2} = \omega_P d_P , \tag{1}$$

where ω_S is the angular speed of the sun, which is the input shaft of the stage, d_S is the diameter of the sun, ω_p is the angular velocity of the planets, and d_p is the diameter of the planets. From Eq. (1) the angular velocity of the planets is,

$$\omega_P = \frac{\omega_S d_S}{2d_P}. \tag{2}$$

Again, from simple kinematics considerations the velocity of point O (v_O), the center of the planets, is given by:

$$v_O = \omega_P \frac{d_P}{2} = \frac{\omega_S d_S}{4}. \tag{3}$$

As the center of the planets are linked to the arm, the angular velocity of the arm (ω_b) is given by:

$$\omega_b = \frac{v_O}{r_b} = \frac{\omega_S d_S}{2(d_p + d_S)}, \tag{4}$$

where r_b is the arm radius.

As the output shaft for each stage is the arm, the transmission ratio for one stage (i) is given by:

$$i = \frac{\omega_S}{\omega_b} = \frac{2(d_P + d_S)}{d_S}. \tag{5}$$

The transmission ratio defined for the speed reducer is 1:81, with each stage responsible for an equal transmission ratio of 1:9. Thus, the relation between the diameters of the planets and the sun obtained from Eq. (5) is the following:

$$9 = \frac{2(d_P + d_S)}{d_S} \Rightarrow d_p = 3.5 d_S. \tag{6}$$

Adopting for the sun a diameter equals to 10mm results into planets with diameters of 35mm and an external ring with diameter of 80mm.

3. The two-stage planetary traction reducer design

Since the dimensions of the sun, planets and external ring are defined from kinematics and dimensional considerations, the design of the traction planetary reducer is limited to determine its life given a required output torque. This section presents the equations used to calculate the forces and stresses applied in the reducer elements, and the life calculation. As the dimensions of the elements of both stages are the same an the torque applied in the second stage is greater in the first stage, only the second stage may be considered in the stress and life analysis of the reducer.

3.1. Force analysis

In a traction speed reducer the maximum output torque is function of the normal forces between the elements in contact. Therefore, the relation between the maximum torque transmitted and the required normal force between the planets and the sun is essential for the design process. Since there are three planets in contact with the sun, the input torque in the second stage of the reducer (T_{e2}) is given by:

$$T_{e2} = \frac{3}{2} F_{Pt2} d_S, \tag{7}$$

where F_{Pt2} is the tangential force in the planets of the second stage. The tangential force in the planets is related to the normal force (F_{Pn2}) by the traction coefficient (μ) according to:

$$F_{Pt2} = \mu F_{Pn2}. \tag{8}$$

Substituting Eq. (8) into (7) results into an expression for the input torque in the second stage as function of the normal force in the planets, i.e.,

$$T_{e2} = \frac{3}{2} \mu F_{Pn2} d_S. \tag{9}$$

Assuming that there is no energy loss in the reducer, the input torque in the second stage can be related to the output torque (T_s) through the transmission ratio of the second stage, i, i.e., $T_s = T_{e2}i$. Thus, the normal force in the contact between the planets and the sun of the second stage as function of the output torque is given by:

$$F_{Pn2} = \frac{2T_s}{3\mu d_S i}. \tag{10}$$

3.2. Stress distribution and contact fatigue

Since normal forces press the elements of the reducer to guarantee their contact the Hertz contact stress theory forms the basis to calculate these elements. However, the Hertz contact stress theory is applied only for static conditions and pure rolling (without sliding) between two surfaces. When rooling is accompanied by sliding the stress field is distorced by the tangential force (the traction force in the case of the traction reducer). Smith and Lui (1953) developed an anlysis including the effects of the tangential force over the stress distribution in the contact region. They concluded that the tangential force has a significant effect on the stress field and the stresses can be separated into normal and tangential components.

The theory presented in this section is taken from Norton (1998) and from Smith and Lui (1953). Nagahashi (2002) performed a study where he verified that the principal stresses appear at the surface of the contact region. Therefore, the equations presented here are for the stresses at the surfaces in contact and are specialized for the case of cylindrical bodies.

For two cylindrical bodies pressed by a normal force, the contact region assumes a rectangular format as shown in Fig. (3).

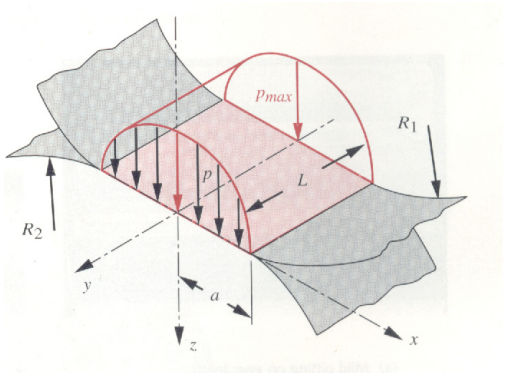

Figure 3. Pressure distribution and contact region formed between two cylindrical bodies in contact (Norton, 1998).

The half of the width of the contact region (a) is given by the following expression:

$$a = \sqrt{\frac{2F_n}{\pi L}\left(\frac{m_1 + m_2}{B}\right)}, \tag{11}$$

where F_n is the normal force, L is the length of the contact region, B is a geometric constant, and m_1 and m_2 are functions of the material of the cylinders. For two cylinders in contact the parameter B is given by:

$$B = \frac{1}{2}\left(\frac{1}{R_1} + \frac{1}{R_2}\right), \tag{12}$$

where R_1 and R_2 are the radius of the two cylinders. The parameters m_1 and m_2 are expressed by:

$$m_1 = \frac{1-\nu_1^2}{E_1}; \qquad m_2 = \frac{1-\nu_2^2}{E_2}; \tag{13}$$

where ν_1 and ν_2 are the Poisson coefficients, and E_1 and E_2 are the Young Modulus of the materiais of cylinders 1 and 2 respectivelly.

The maximum contact pressure (p_{max}) is related with the normal force and the width of the contact region according to the following expression:

$$p_{\max} = \frac{2F_n}{\pi a L}. \tag{14}$$

For points at the surface the stresses due to the normal force are calculated by the following expressions:

$$\sigma_{zn} = \sigma_{xn} = \begin{cases} -p_{\max}\sqrt{1-\dfrac{x^2}{a^2}}, & \text{for} \quad |x| \le a; \\ 0, & \text{for} \quad |x| > a. \end{cases} \tag{15}$$

The stresses due to the tangential force for points at the surface are the following:

$$\sigma_{xt} = \begin{cases} -2f_{\max}\left(\dfrac{x}{a} - \sqrt{\dfrac{x^2}{a^2}-1}\right), & \text{for} \quad x \ge a; \\ -2f_{\max}\left(\dfrac{x}{a} + \sqrt{\dfrac{x^2}{a^2}-1}\right), & \text{for} \quad x \le -a; \\ -2f_{\max}\dfrac{x}{a}, & \text{for} \quad |x| \le a; \end{cases}$$

$$\tau_{xzt} = \begin{cases} -f_{\max}\sqrt{1-\dfrac{x^2}{a^2}}, & \text{for} \quad |x| \le a; \\ 0, & \text{for} \quad |x| > a; \end{cases} \tag{16}$$

where f_{max} is the maximum tangential pressure defined as $f_{\max} = \mu p_{\max}$.

Adding the stresses due to the normal and tangential forces results into the total stresses in the x, y and z directions as follows:

$$\begin{aligned} \sigma_x &= \sigma_{xn} + \sigma_{xt}; \\ \sigma_z &= \sigma_{zn} + \sigma_{zt}; \\ \sigma_y &= \nu(\sigma_x + \sigma_z); \\ \tau_{xz} &= \tau_{xzn} + \tau_{xzt}. \end{aligned} \tag{17}$$

Note that the normal stress σ_{zt} and the shear stresses τ_{xzn}, τ_{xy} and τ_{yz} are always zero at the surface for any point in the region of contact.

The principal stresses σ_1, σ_2 and σ_3, which are used to calculate the life of the surfaces in contact, are given by the eigen-values of the stress tensor matrix, defined as:

$$[T] = \begin{bmatrix} \sigma_x & \tau_{xy} & \tau_{xz} \\ \tau_{xy} & \sigma_y & \tau_{yz} \\ \tau_{xz} & \tau_{yz} & \sigma_z \end{bmatrix}. \tag{18}$$

The maximum shear stress, τ_{13}, is given by:

$$\tau_{13} = |\sigma_1 - \sigma_3|/2, \tag{19}$$

where σ_1 and σ_2 are largest and smallest principal stresses respectively.

Below the surface the compression stresses due to the normal force decrease. However, the shear stress increases bellow the surface reaching a maximum at a deepth equals to $0.5a$. The peak to peak value of the shear stress due to the normal force is $0.5p_{max}$ for any traction coefficient.

The main failure mechanisms for surfaces in contact are wear and pitting. Some authors consider that the peak to peak value of the shear stress is responsible for most of the failure that happens below the surface. However, there is a big controversy about which is the most important failure mechanism and also about the location of the failure.

Nevertheless there exists a consensus that the largest principal stress is the one that shall be compared to the fatigue limit of the material to determine the life of surfaces in contact.

The following expression determines the life of surfaces in contact:

$$N = 10^{(\zeta - \lambda \log_{10} k)}, \tag{20}$$

where N is the number of cycles until failure, ζ and λ are the resistance factors of the material, and k is the experimental load factor given by:

$$k = \pi (m_1 + m_2) \sigma^{2}_{\text{princ\_máx}}, \tag{21}$$

where $\sigma_{\text{princ\_máx}}$ is the maximum principal negative (compression) stress. In Eq. (21) the unit used for stress is psi.

Analysing Eq. (15) and (16), associated with Eq. (11), (12) and (14), it may be observed that the largest stresses will appearin the contact between the sun and the planets due to the smallest radius of theses elements. In the planetary traction reducer, for each turn of the output shaft, a given point of the sun of the second stage is submitted to 3 loads due to the presence of 3 planets. Thus, the sun is the most solicited element of the reducer.

3.4. Calculation of the reducer life

For calculation of the reducer life the following data are adopted:

- The diameters of the sun and planets are 10mm and 35mm respectively;
- The material of the sun is 8620 cemented steel with surface hardness 60 HRC;
- The material of the planets is AISI 52100 steel with surface hardness 197 HRC;
- The transmission ratio per stage is 9;
- The Poisson coefficient and Young Modulus of the sun and planets materials are 0.3 and 207GPa respectively;
- According to the study made by Kraus (1992) the estimated traction coefficient provided by the Santotrac-50 for the operating conditions presented in the reducer is 0.06;
- According to Morrison (1968), considering rolling with 9% of sliding, for the material used for the sun the fatigue factors are: k = 12700psi, λ = 7.39, and ζ = 38.33.

The reducer life is function of the maximum output torque. Figure (4) shows the principal stresses, the Von Misses stress (σ_{VM}) and the maximum shear stress in the sun as function of the distance from the center of the contact region, and Tab. (1) presents a summary of the calculation results for three different output torques. The normal force applied to the sun and planets to transmit a desired output torque is calculated from Eq. (10). The maximum contact pressure is calculated from Eq. (11), (12), (13) and (14). The principal stresses are calculated as function of the distance from the center of the contact using Eq. (15), (16), (17), (18) and (19). Giving the maximum principal stress the reducer life is calculating using Eq. (20) and (21).

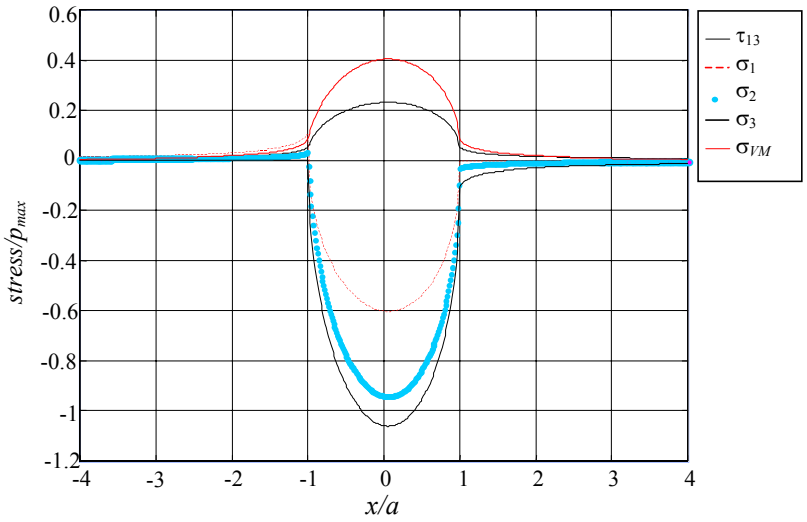

Figure 4. Distribution of principal stresses, Von Mises stress and maximum shear stress in the contac region.

Fig. (4) shows that the stress distribution is not symmetric around the center of contact; this is caused by the presence of the tangential force. Also, observe that the maximum principal stress is greater than the maximum contact pressure; again this is caused by the tangential stress component that is added to the normal stress component to form the total stress.

Table 1. Summary of the calculation of the reducer life.

Output Torque (Nm)	Normal force (N)	Maximum contact pressure (N/m^2)	Maximum principal stress (N/m^2)	Estimated life (number of cycles of the output shaft)
30	3703.7	1472.6	1563.6	$8.0x10^7$
40	4938.3	1700.4	1805.4	$1.8x10^6$
50	6172.8	1901.0	2018.5	$9.4x10^4$

Observe that the results for the reducer life presented in Tab. (1) are calculated considering that there is metal-to-metal contact between the sun and the planets. Since the metal-to-metal contact is avoided by the presence of the Santotrac-50 film pad between the elements, the actual life of the reducer will be greater than this calculated value. This was done because no data was found for the fatigue factors for the case of contact using Santotrac-50.

4. Pre-load system

To apply the required normal force to obtain the desired output torque, a pre-load system as shown in Fig. (5) is used. This system is composed by two rings with conical formats and several screws. When the conical surfaces are approximated by the screws a pressure is applied on the external ring and on the body of the reducer. The pressure on the external ring is transmitted to the planets and the sun, resulting in the required normal force.

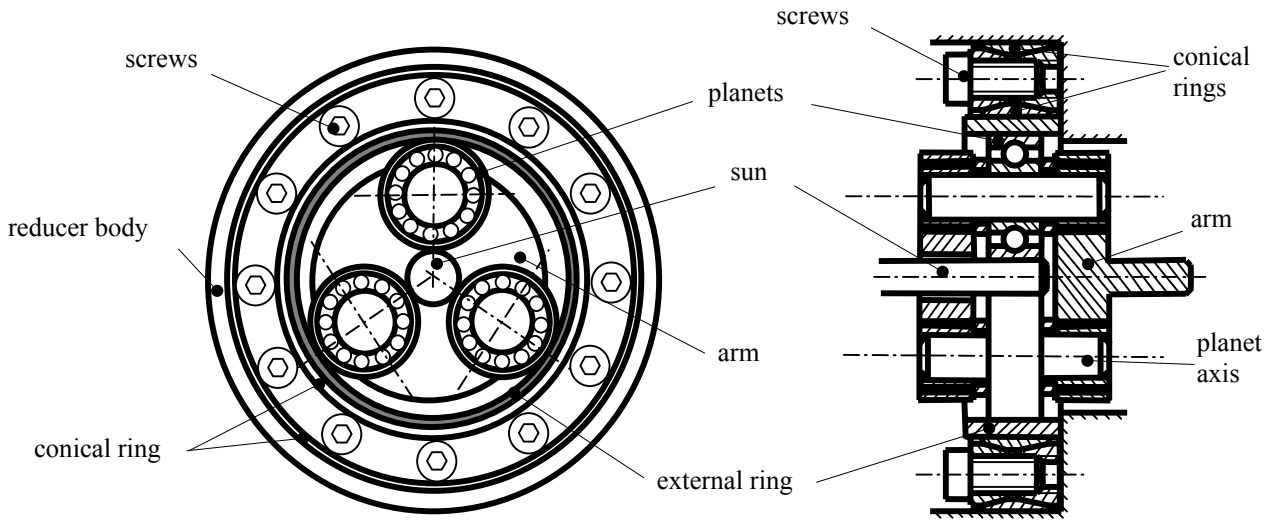

Figure 5. Frontal and lateral views of the pre-load system.

The arms have cuts and holes around the positions where the planets' axes are fixed. These cuts and holes allow small radial movements of the planets' axes. The radial movements permit applying the pre-load force without causing stresses due to the deformation of the planets' axes, and also make simpler the assembly process. Figure (6) shows a frontal view of the arm showing the cuts and holes.

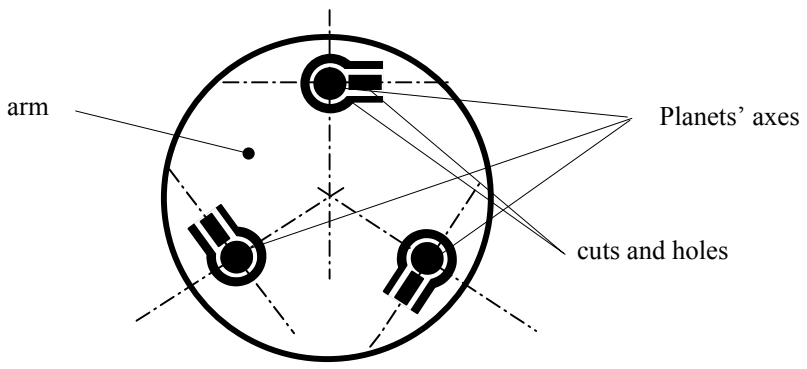

Figure 6. Frontal view of the arms showing the cuts and holes around the planets axes.

5. Tests and results

The following characteristics of the speed reducer were calculated through experimental tests to verify its performance:

- Angular transmission error;
- Angular velocity fluctuation;
- Backlash;
- Torsional stiffness.

The experimental apparatus used to test the reducer is described in details in Nagahashi (2002), this apparatus is similar to the one used by Mitsubishi (19__) to test its high precision speed reducers. The speed reducer is driven by a DC electric motor through a flat belt. The flat belt is used to minimize vibrations that may be caused by the motor to be transfer to the reducer. To measure the angular positions of the input and the output shafts optical encoders are used with resolutions of 36 and 18 seconds of arc respectively.

The experimental results presented in this section are obtained with a pre-load force required for an maximum output torque of 30Nm. Figure (7) presents a typical result for the angular velocities for the input and output shafts for clockwise rotation. All the tests are preformed with the motor at constant angular velocity. Since optical encoders are used to measure the angular position, the angular velocity is calculated as follows:

$$\omega = \frac{\theta(t+T) - \theta(t)}{T}, \tag{22}$$

where ω is the angular velocity of the input or the output shaft, θ is the angular position read from the encoder, and T is the sampling period, i.e., the time interval between two consecutive readings of the encoder's counter.

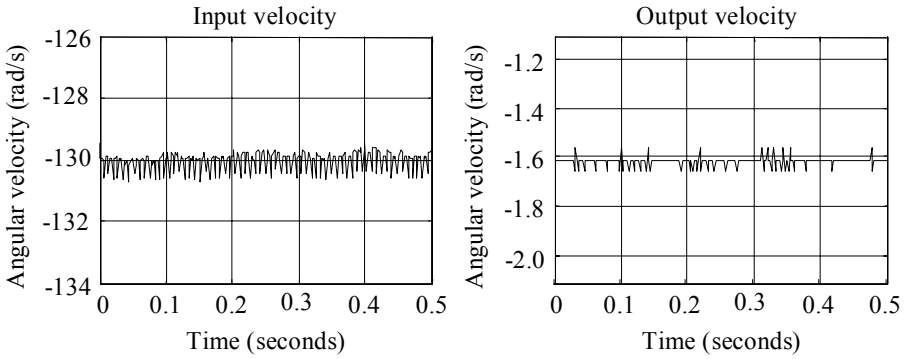

Figure 7. Experimental data for the angular velocity for the input and output shafts for clockwise rotation.

Figure (8) presents the angular transmission error and the angular velocity fluctuation calculated using the data shown in Fig. (7).

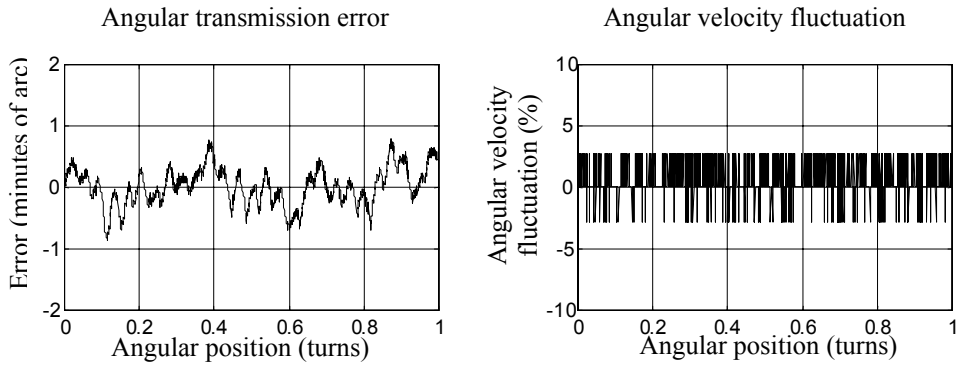

Figure 8. Calculated values for the angular transmission error and the angular velocity fluctuation for one turn of the output shaft for clockwise rotation.

The angular transmission error ($d\theta$) is calculated from experimental data according to the following equation:

$$d\theta = \theta_2 - \theta_1 / i_T, \tag{23}$$

where θ_1 and θ_2 are the angular position of the input and output shafts respectively, and i_T is the total transmission ratio of the speed reducer. The angular velocity fluctuation is calculated using experimental data as follows:

$$\delta = \frac{\Delta\omega}{\omega_2} = \frac{\omega_2 - \omega_1 / i_T}{\omega_2}, \tag{24}$$

where δ is the rate of the angular velocity fluctuation, $\Delta\omega$ is the angular velocity fluctuation, and ω_1 and ω_2 are respectively the angular velocity of the input and output shafts.

The results of angular velocity and angular velocity fluctuation show small oscillations typical of quantization errors. The encoder used to measure the angular position of the output shaft does not have the adequate resolution. An encoder with resolution of at least 5 seconds of arc would be necessary to eliminate these quantization errors. Thus, from the measurements of angular velocity fluctuation it is not possible to conclude if these fluctuations are caused by the reducer operation. Table (2) presents a summary of the results obtained from several tests with the speed reducer. Observe that the error between the measured transmission ratio (1:80.62) and the nominal value (1:81) is very small, about 0.5%.

Table 2. Results for the angular transmission error and the angular velocity fluctuation.

Measured transmission ratio	80,62
Angular transmission error (minutes of arc)	1,5
Angular velocity fluctuation (rad/s)	less than 0,09
Rate of angular velocity fluctuation (%)	less than 5,57%

To determine the backlash and the torsional stiffness the input shaft is blocked and torque is applied at the output shaft. The torque is applied in the following sequence: (1) starting from zero the torque is increased up to 50% of the maximum torque in one direction; (2) then, the torque is gradually decrease until returning to zero; (3) the torque is now applied in the other direction following the same procedure, i.e., it is increased from zero to 50% of the maximum torque and then gradually decreased to zero. For each value of torque the angular position of the output shaft and the torque itself are measured. Figure (9) presents a typical result obtained in this test where it is possible to observe that the reducer presents no backlash. A backlash would be represented by a discontinuity (large horizontal variation) in the angular position when the applied torque changes its direction, i.e., when the torque passes through zero. The variation of the angular position is different during the load and the unload stages of the test, causing a small hysteresis. This hysteresis is caused by a small amount of sliding between the rolling surfaces. The torsional stiffness of the traction planetary reducer is given by the tangent of the curve of the angular position versus torque, resulting in a value about 2,5 Nm/min.

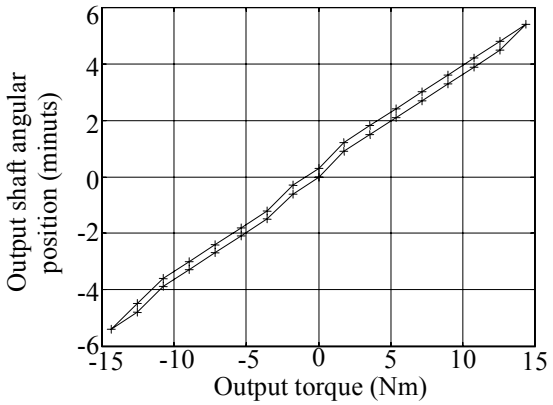

Figure 9. Typical result for the test of torsional stiffness.

For comparison purposes Tab. (3) presents a classification of speed reducers according to their precision, as given by Mitsubishi (19__).

Comparing the information given by Tab (3) with the results obtained for the traction planetary reducer it is possible to conclude the following:

- The results of angular transmission error classifies the reducer as belonging to the precision class;
- The results of backlash allows to classify the reducer as belonging to the high precision class;
- Due to the quantization errors the results of angular velocity fluctuation cannot be used to classify the reducer according to the precision.

Table 3. Classification of speed reducers according to the precision (Mitsubishi, 19__).

Parameter	High Precision	Precision	Normal
Rate of angular speed fluctuation (δ - %)	$\delta < 0{,}2\%$	$0{,}2\ \% < \delta < 3{,}0\ \%$	$\delta > 3{,}0\ \%$
Angular transmission error ($d\theta$ - seconds of arc)	$d\theta < 50$	$50 < d\theta < 100$	$d\theta > 100$
Backlash ($C\theta$ - minutes of arc)	$C\theta < 2$	$2 < C\theta < 10$	$C\theta > 10$

6. Conclusions

In this work a traction planetary speed reducer has been designed and test. The reducer presents zero backlash and an angular transmission error small enough to be classified as a precision reducer. Although it was not possible to measure with the required resolution the angular velocity fluctuation is observed to be very small.

The measured transmission ratio is slightly different than the nominal value. This ratio was measured with no load applied to the output shaft and the difference, which is about 0.5%, is probably caused by the presence of sliding during the operation.

The stiffness of the reducer is relatively low, about 50% lower than the stiffness of a precision gear reducer with the same maximum output torque and about the same weight. The reducer stiffness in highly affected by the normal force applied to generate the traction force. Giving a desired life the normal force is limited by the diameter of the sun, thus, the stiffness of the traction reducer may be enhanced by increasing the sun diameter.

It is important to observe that the reducer life is calculated considering that there is metal-to-metal contact between the sun and the planets. Since the metal-to-metal contact is avoided by the presence of the Santotrac-50 the actual life of the reducer is greater than the calculated value. A more realistic value for the reducer life was not possible to calculated due to the lack of data concerning contact fatigue factors in the presence of Santotrac-50. Also, note that a sliding of 9% was assumed to calculate the reducer life and this value is greater than it was observed.

Future work is underway to measure the angular velocity fluctuation without quantization problems and the maximum output torque. The measurement of the maximum output torque is important because all the calculations are based on this torque. Finally, to conclude this work it is still necessary to measure experimentally the real life of the reducer under operating conditions to validate the calculations performed.

7. References

Cisneros, C. A. F., 1996, “Design of a Composed Planetary Traction Speed Reducer”, Master Dissertation, Department of Mechanical Engineering, Escola Politécnica da USP, São Paulo, Brazil (in Portuguese).

Hunold, M. C., 1999, “Rotative Pneumatic Positioning System”, Doctoral Thesis, Department of Mechanical Engineering, Escola Politécnica da USP, São Paulo, Brazil (in Portuguese).

Kraus, C. E., 1985, “Rolling Traction Analysis and Design”,. Excelermatic Inc., Texas, USA.

Loewenthal, S. H. and Rohn, D.A., 1985, “Elastic Model of the Traction Behavior of Two Traction Lubricants”, ASLE Transactions, v.27,2, pp.129-137.

Morrison, R. A., 1968, “Load/Life Curves for Gear and Cam Materials”, Machine Design, Vol. 40, pp. 102-108.

Mitsubishi, 19__, “Rotation Accuracy of Mitsubishi Planetary Traction Drive Unit”, Tokyo, Japan.

Nagahashi, F. S., 2002, “Design, Construction and Test os a Two-Stage Planetary Traction Speed Reducer”, Master Dissertation, Department of Mechanical Engineering, Escola Politécnica da USP, São Paulo, Brazil (in Portuguese).

Norton, R. L., 1998, “Machine Design: An Integrated Approach”, Prentice-Hall, New Jersey.

Smith, J. O. and Lui, C.K., 1953, “Stresses Due to Tangential and Normal Loads on an Elastic Solid with Application to Some Contact Stress Problems”, Journal of Applied Mechanics. Transactions of The ASME, 75: pp.157-166.

Nagahashi, F. S., “Design, Construction and Tests of a Tw-Stage Planetary Traction Speed Reducer”, Master Dissertation, Department of Mecatronic Engineering, Escola Politécnica da USP, São Paulo, Brazil (in Portuguese).